Assessing the hydrological impacts of climate change in the headwater catchment of the Tarim River basin, China

Zhaofei Liu, Zongxue Xu, Guobin Fu and Zhijun Yao

ABSTRACT

Two statistical downscaling models were used to downscale regional climate change scenarios, on the basis of the outputs of three general circulation models (GCMs) and three emission scenarios. Driven by these climate change scenarios, a distributed macro-scale hydrological model (the Variable Infiltration Capacity (VIC) model) was applied to assess the impact of climate change on hydrological processes in the headwater catchment (HC) of the Tarim River basin, China. The results showed that the HC tends to experience warmer and drier conditions under the combined climate change scenarios. The predictions show a decreasing trend of the runoff in the HC, driven by the combined climate change scenarios. The results predicted an increasing trend for winter runoff however, which was consistent with the forecasts from most previous studies on other locations such as the region of St Lawrence tributaries (Quebec, Canada) and the Willamette River Basin (Oregon, USA). There was an inconsistent intra-annual distribution of the changes in precipitation and runoff in the HC; these inconsistencies may be explained by increasing snowmelt runoff resulting from higher air temperature. It was concluded that uncertainties within different GCM outputs are more significant than emission scenarios in the assessment of the potential impact of climate change.

Key words | GCM, Non-homogeneous Hidden Markov Model (NHMM), runoff, Statistical Downscaling Model (SDSM), Special Report on Emission Scenarios, VIC model

Zhaofei Liu
Zhijun Yao
Institute of Geographic Sciences and Natural Resources Research,
Chinese Academy of Sciences,
Beijing 100101,
China

Zhaofei Liu
Zongxue Xu (corresponding author)
Key Laboratory of Water and Sediment Sciences,
Ministry of Education,
College of Water Sciences,
Beijing Normal University,
Beijing 100875,
China
E-mail: *zongxuexu@vip.sina.com*

Guobin Fu
CSIRO Land and Water,
Private Bag 5,
Wembley WA 6913,
Australia

INTRODUCTION

On the basis of past greenhouse gas emissions and inertia in socioeconomic systems, it is anticipated that future climate change is unavoidable and that adaptation will become necessary. Climate change is likely to produce significant effects on the hydrological cycle through global-warming-induced changes in snow and ice cover, changes in precipitation patterns and changes in soil moisture and runoff. Although there is considerable uncertainty in the projected patterns of precipitation at the regional scale, the Intergovernmental Panel on Climate Change (IPCC) fourth report (AR4) suggests that precipitation and average annual river runoff are likely to increase in the mid-latitudes and some areas in the humid tropics, but likely to decline in many semiarid regions (Solomon *et al.* 2007). However, given that the adaptation policy tends to be made at national, regional and local levels, there is a need to assess the impact of climate change on hydrological processes and water resources at these scales.

General circulation models (GCMs) are the primary tool for generating climate change scenarios (Murphy *et al.* 2004; Solomon *et al.* 2007; Andersson *et al.* 2011). However, the GCM simulation of local climate on spatial scales smaller than the original GCM grid cells is often poor, especially when the area has complex topography (Schubert 1998; McAvaney *et al.* 2001). Downscaling to generate information below the grid scale of GCMs is therefore necessary. There are two main approaches to downscaling: dynamical and statistical (Fowler *et al.* 2007). Fowler *et al.* (2007) reviewed downscaling techniques and found that dynamical downscaling methods provide little advantage over statistical techniques. Murphy (1999) also pointed out that although dynamical and statistical downscaling (SD) methods

doi: 10.2166/nh.2012.237

generate similar reproduction of current climate (Wilby *et al.* 2000), they can differ significantly in the projection of future climate conditions. SD was used in the present study since this method offers considerable computational savings and can be relatively easily applied to different GCMs, parameters and regions (Cubasch *et al.* 1996; Timbal *et al.* 2003; Wilby *et al.* 2004; Wood *et al.* 2004).

SD methods can be classified into three types (Wilby *et al.* 2004), namely those that involve regression models (transfer functions), weather generators and weather classification. In general, SD methods that combine multi-techniques are possibly the most appropriate (Christensen *et al.* 2007). The Statistical Downscaling Model (SDSM) includes deterministic transfer functions and stochastic components (Wilby *et al.* 2002), while the Non-homogeneous Hidden Markov Model (NHMM) includes weather classification, regression and stochastic components (Charles *et al.* 1999). Liu, L. L. *et al.* (2011) and Liu, Z. F. *et al.* (2011) found that the NHMM model performed better than SDSM in downscaling the daily precipitation over the Tarim River basin (TRB). The NHMM was only developed for downscaling precipitation. Therefore, both NHMM and SDSM were selected; NHMM was used to downscale precipitation and SDSM to downscale air temperature.

Although a few previous studies employed empirical methods (e.g. Teegavarapu 2010; Zeng *et al.* 2011), hydrological models had advantages for use in the assessment of the impacts of future climate change on local hydrology (Gleick 1986; Singh & Kumar 1997). Many different hydrological models, including the Variable Infiltration Capacity (VIC) model, have been used previously (Beyene *et al.* 2010; Elsner *et al.* 2010; Maurer *et al.* 2010). It is important to identify whether simple or complex models should be used for selecting a suitable model (Jiang *et al.* 2007). There are many factors involved in the choice of a model for a particular study (Gleick 1986), in which the dominant factors include the purpose of study and model and data availability (Xu 1999). Given that the main purpose of this study is to assess the hydrological impacts of climate change in a macro-scale basin, a macro-scale hydrological model, namely the VIC model (Liang *et al.* 1994, 1996), was used. The VIC model has been widely used at large scales, and it has also been used for studies for the arid regions in China (Su & Xie 2003; Xie *et al.* 2004).

Overall, the method that uses climate change scenarios downscaled from GCM outputs to drive hydrological models is the most useful method for assessing the impacts of future climate change on regional hydrology. Further, on the basis of multi-GCMs and multi-emission scenarios, climate projections can provide an uncertainty envelope for the projected runoff. These methods have been widely applied in recent studies of different countries and regions, including: the USA (Maurer *et al.* 2010; Lan *et al.* 2011); Canada (Chen *et al.* 2011; Kehta *et al.* 2012); the Itaipu Basin located on the frontier between Brazil and Paraguay (Sosa *et al.* 2011); Ethiopia (Abdo *et al.* 2009); Sweden (Teutschbein *et al.* 2011); Ireland (Bastola *et al.* 2011); the Greater Caucasus (Hagg *et al.* 2010); South Africa (Graham *et al.* 2011); Australia (Chiew *et al.* 2010); Iran (Khazaei *et al.* 2011); and Korea (Bae *et al.* 2011). In general, there are large differences between future runoff scenarios under different climate change projections for different regions. All of these studies projected an increasing trend for air temperature, and most of them predicted an increasing trend for winter runoff (e.g. Boyer *et al.* 2010; Chang & Jung 2010; Chen *et al.* 2011; Forbes *et al.* 2011; Liu, L. L. *et al.* 2011; Liu, Z. F. *et al.* 2011; Kienzle *et al.* 2012), which was mainly attributed to more snowmelt runoff caused by warmer winters. In the case of China, several studies estimated the impacts of climate change on the local hydrology in some regions, including the Yellow River basin (Liu, L. L. *et al.* 2011; Liu, Z. F. *et al.* 2011), the Yangtze River basin (Zeng *et al.* 2011), the Songhua River basin (Meng & Mo 2012), the TRB (Liu *et al.* 2010) and the Poyang Lake region (Ye *et al.* 2011). These studies however lacked hydrological models, did not use downscaling methods or used only one GCM. Few previous studies have used multi-GCM outputs, downscaling methods and hydrological models to assess potential impacts of climate change on hydrology at the basin scale in China.

In this study, multi-GCMs and multi-emission scenarios were downscaled for regional climate projections, which could represent an uncertainty envelope for impact assessment. Multiple climate change scenarios were used to drive the VIC model to assess the impact of future climate change on hydrological processes in the headwater catchment (HC) of the TRB. Runoff is more sensitive to climate change in arid regions than in humid regions. Therefore, an

assessment of the impact of climate change on water availability in arid regions is of great scientific and practical importance to water resource management in the arid regions of the world. The TRB is the largest inland river basin (1.02×10^6 km^2) in China. It is characterized as having an extremely dry desert climate, with little precipitation and strong potential evaporation (Xu *et al.* 2010). The TRB is rich in natural resources, but the ecological environment in the basin is extremely vulnerable due to very limited water resources (Chen *et al.* 2006; Liu *et al.* 2010). The variability and availability of water resources have direct influences on local eco-environmental conservation and sustainable socioeconomic development (Zhang *et al.* 2010).

STUDY AREA

The TRB, located at 73–97° E and 34–45° N, is the largest inland river basin in China (Figure 1). It is situated in southern Xinjiang Autonomous Region and includes five autonomous states and 42 cities (Xu *et al.* 2010). The basin area of 1,020,000 km^2 includes nine sub-basins, the mainstream region, the Taklamakan Desert and eastern desert regions (Xu *et al.* 2010). Historically, nine rivers have been hydraulically connected to the Tarim River mainstream. At present however, only four rivers have maintained a hydraulic connection to the mainstream. Three of these, namely the Akesu, Yerqiang and Hetian rivers, have hydraulic connections with the upstream Tarim River. As shown in Figure 1, the HC of the TRB can be regarded as a single catchment with relatively independent hydrological units; it was therefore selected as the study area. The catchment has distinct runoff generation characteristics. Annual precipitation in the plain region is usually less than 100 mm; runoff is therefore not generated. Runoff is only generated in the high mountainous region, but it is consumed in the low plain region due to evaporation or irrigation.

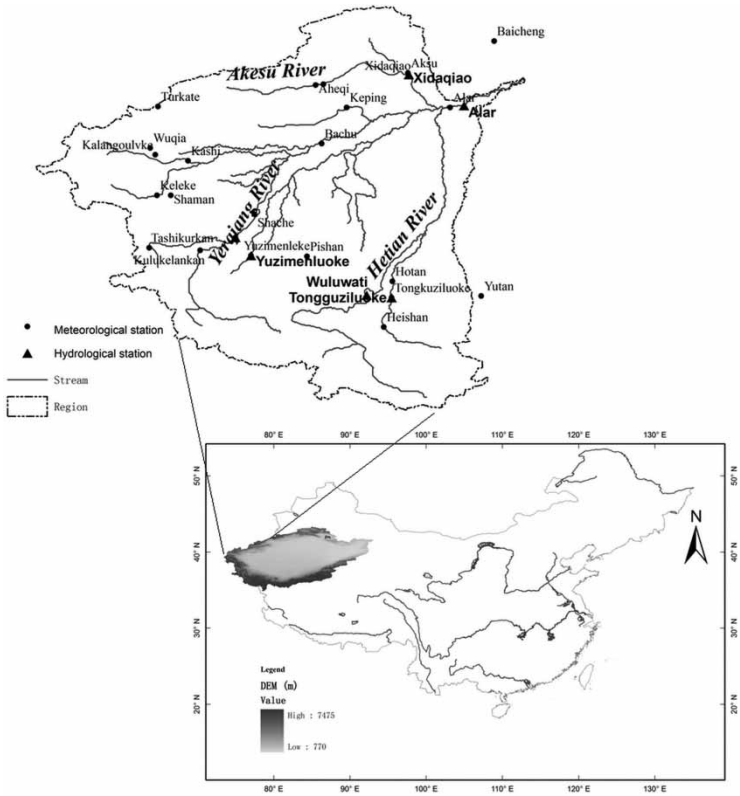

Figure 1 | Location of the TRB in northwest China and meteorological stations. The right panel shows the location and digital elevation model of the TRB in China. The left panel shows the headwater catchment of the TRB.

DATASET DESCRIPTION

Observed stations data

Observed daily data series for the period 1961–2010 were obtained from 14 National Meteorological Observatory (NMO) stations located in or around the TRB (see Figure 1); the data series included data on precipitation, maximum air temperature (T_{max}), minimum air temperature (T_{min}) and mean wind speed (National Climatic Centre of China). Another 10 precipitation stations and five hydrological stations with daily data series of precipitation and monthly streamflow were also selected; these stations were maintained by the Bureau of Hydrology, China Ministry of Water Resources. The sum of the streamflow from five hydrological stations (Figure 1) were considered as the total discharge of the HC rather than the streamflow at Alar station, which was the control station for the catchment. This was because the streamflow at Alar station had been greatly changed by human activities such as those related to reservoirs and irrigation. Observed streamflow data was only available for several non-consecutive series, which include monthly series for 1964, 1971, 1976–1979, 1981, 1983–1984, 1986–1987 and 2001–2005.

NCEP reanalysis data

The National Center for Environmental Prediction and National Center for Atmospheric Research (NCEP/NCAR) reanalysis datasets (Kalnay *et al.* 1996; Kistler *et al.* 2001) for the period 1961–2000, containing the suite of daily atmospheric variables, were selected as observed large-scale predictors. Both pressure and surface variables were selected as candidate predictors; these predictors include five pressure variables at three pressures (400 hPa, 500 hPa, 600 hPa) and five surface variables. These three pressures were selected because data for pressures greater than 600 hPa were not available from the GCM outputs in the study area. The candidate predictors include circulation-related predictors and humidity variables. Circulation-related predictors are usually selected as candidate predictors because GCMs were shown to accurately simulate these predictors (Cavazos & Hewitson 2005). In addition, humidity variables are useful to downscale precipitation (e.g. Karl *et al.* 1990; Murphy 1999; Wilby & Wigley 2000), especially as it may be an important predictor under a changed climate.

GCM outputs

Three GCMs, namely CSIRO30, ECHAM5 and GFDL21, were selected for use in this study. Detailed information about these models can be found at the IPCC Data Distribution Centre website (http://ipcc-ddc.cru.uea.ac.uk). Three emission scenarios of the IPCC Special Report on Emissions Scenarios (SRES), namely A1B, A2 and B1, were selected for each of the GCMs. SRES A2, A1B and B1 simulations represented the higher, medium and lower emission scenarios, respectively (Christensen *et al.* 2007). The data series included both the present control period (1961–2000) and two future periods (2046–2065 and 2081–2100).

SRES A1B describes a future world with rapid economic growth, global population that peaks at mid-century and declines thereafter and the rapid introduction of new and more efficient technologies based on the balance of all energy sources. SRES A2 describes a very heterogeneous world with a continuously increasing population, economic development that is primarily regionally oriented and technological change that is more fragmented and limited than in the other scenarios. SRES B1 scenario envisages a convergent world with the same global population pattern as SRES A1B but with rapid change in the economic structures, reduction in material intensity and the introduction of clean and resource-efficient technologies. More details about the SRES are available in the IPCC AR4 (Christensen *et al.* 2007).

DEM, soil and land cover data

Shuttle Radar Topographic Mission (SRTM) Digital Elevation Model (DEM) data for the TRB were obtained from the SRTM website (http://srtm.csi.cgiar.org). Spatial soil data with a resolution of $30' \times 30'$ were derived from the ISRIC-WISE soil database (http://www.isric.org). The soil database considered 22 soil variables that were identified as being useful in agro-ecological zoning, land evaluation, crop-growth simulation, modelling of soil gaseous emissions and analysis of the global environmental

change. Soil texture data were reclassified into 12 texture categories according to the United States Department of Agriculture (USDA). The University of Maryland's 1 km global land cover data, obtained from the Advanced Very High Resolution Radiometer (AVHRR; available from http://glcf.umiacs.umd.edu/data/), were used. All the pixels were used within a hierarchical tree structure to classify the AVHRR data into 12 classes.

STATISTICAL DOWNSCALING MODELS

SDSM

The SDSM is a hybrid model involving a combination of the stochastic weather generator and multi-linear regression methods. This approach is used because regional circulation patterns and atmospheric moisture variables are used to condition the local precipitation at each station (Harpham & Wilby 2005). The regression component represents the deterministic part of the model, while the stochastic component represents the random element of the model (Prudhomme & Davies 2009). The multi-linear regression of the model is used to derive a statistical relationship between the predictors and precipitation, and the model includes some transform functions in order to obtain secondary data series of the precipitation and predictors that have stronger correlations than the original data series. It allows the prediction of local weather conditions from large-scale predictor variables simulated by the GCMs under baseline and changed climatic scenarios. Precipitation is then modelled by the stochastic weather generator, conditioned on predictors. The stochastic component was added to replicate a variance closer to the observed variability because the chaotic nature of local weather conditions cannot be fully explained by the variations in predictor variables. SDSM therefore facilitates multiple simulations with slightly different time-series attributes, but the same overall statistical properties. Full technical details of SDSM may be found in Wilby *et al.* (2002).

NHMM

The NHMM can be defined by a state transition probability matrix and a precipitation occurrence probability distribution (Charles *et al.* 1999). It defines stochastic conditional relationships between multi-site daily precipitation occurrence patterns and a discrete set of weather states, which are referred to as hidden states because they are not directly observable. The transition probabilities between these hidden states, which are conditional on a set of predictors but are not fixed as in the case of homogeneous HMM, are then defined by a first-order Markov chain. Finally, multi-site daily precipitation levels are simulated by conditional multiple linear regression.

Hydrological model

This study used the grid network version of the three-layer VIC (VIC-3L) model (Liang & Xie 2001), a macro-scale hydrology-based land surface model that takes into account both infiltration and saturation excess runoff. The VIC-3L model divides the vertical soil profile into layers comprising an upper layer, a lower layer and a thin layer on top of the upper layer (Liang *et al.* 1996). The upper layer represents the dynamic behaviour of the soil column that responds to rainfall events; the lower layer characterizes the slow variation in between-storm soil moisture behaviour. The thin topsoil layer allows for rapid bare soil evaporation following small summer rainfall events. Horizontally, each grid cell can have partial surface coverage by a number of land cover classes.

The simulated runoff at each grid was routed to the outlet of the catchment (Alar station) using the unit hydrograph method for overland flow (including the surface flow and subsurface flow) and the linear Saint-Venant method for channel flow. The area fraction of each grid was applied in the routing model to deal with the area mismatch between the digital boundary on the basis of the grids and the actual boundary.

MODEL SETTINGS AND EVALUATION CRITERIA

The long observed data series (1961–2000) were split into two periods, 1981–2000 and 1961–1980, which were used for model calibration and validation, respectively. The period 1981–2000 was selected for model calibration because both observed and NCEP datasets contained more

quality data than previous periods. The models calibrated and validated using observed predictors derived from reanalysis data were then driven by predictors derived from large-scale predictor variables simulated by GCMs in the control period (1981–2000) and the future prediction periods (2046–2065 and 2081–2100). Finally, local climate change (daily precipitation and air temperature) scenarios, which include multi-GCMs and multi-emission scenarios, were estimated by the difference between the downscaled variables for the future periods and the control period under the IPCC SRES A1B, A2 and B1 emission scenarios.

The VIC-3L model was applied in the HC of the TRB with a resolution of $0.5^{\circ} \times 0.5^{\circ}$. Either full energy balance and water balance or only water balance were developed in the VIC-3L model. In this study, full energy balance and water balance were adopted to simulate evapotranspiration, runoff and soil moisture. The running step of the model was 24 h. The vegetation, soil and meteorological forcing datasets for each grid cell were applied to the VIC-3L model as model inputs for simulations in the catchment from 1963 to 2005; here, the data series for 1963–1964 were used for model initialization.

Meteorological forcing data, which included daily precipitation, maximum air temperature, minimum air temperature and mean wind speed from 24 stations in the catchment, were interpolated to 203 grids on the basis of the Thiessen polygons method. The non-consecutive observed streamflow data, which included the periods 1960s, 1970s and 1980s, were used for model calibration. The period from 2001 to 2005 was selected for model validation since it contained relatively long, consecutive data series for observed streamflow.

Several criteria were selected to evaluate the performance of the models. Model bias was evaluated according to relative error (RE), which reflected the difference between modelled and observed mean values. Extreme events, which are of interest in climate impact assessments, also need to be reasonably well modelled; hence, the 5th and 95th percentile values of each variable were also

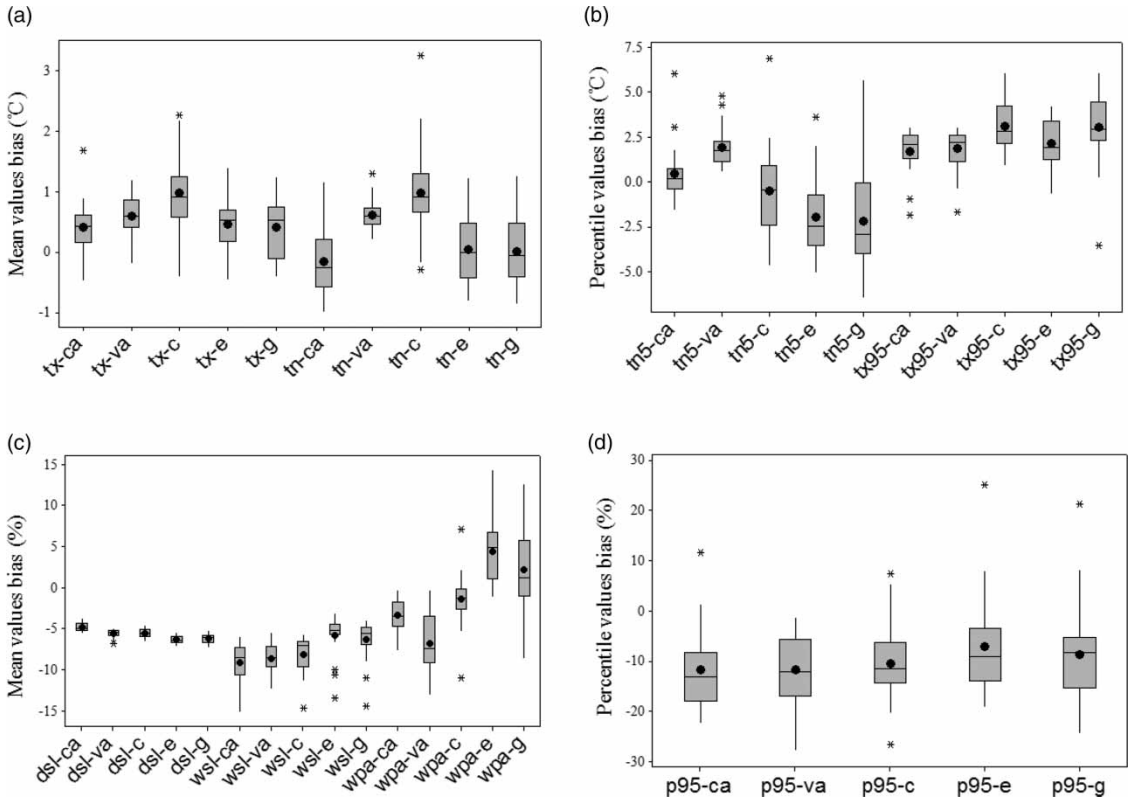

Figure 2 | Model bias for precipitation and temperature. Bias of (a) mean and (b) percentile values for temperature; bias of (c) mean and (d) percentile values for precipitation. –ca, –va refer to calibration and validation, respectively; –c, –e, –g refer to predictors of CSIRO30, ECHAM5 and GFDL21, respectively; tx, tn refer to maximum and minimum air temperatures, respectively; tn5, tx95, p95 mean 5th value of minimum air temperature, 95th value of maximum air temperature and wpa, respectively.

considered. Three variables, namely wet-day precipitation amount (wpa), wet-spell length (wsl) and dry-spell length (dsl) were analysed for precipitation.

Two skill scores, BS and S_{score} based on probability density functions (PDFs), were used to measure how well each model captured the PDFs of each variable; the scores were assessed with daily data series and computed as shown:

$$BS = \frac{1}{n}\sum_{i=1}^{n}(P_{\text{m}i} - P_{\text{o}i})^2 \quad (1)$$

$$S_{\text{score}} = \sum_{i=1}^{n}\text{Min}\,(P_{\text{m}i}, P_{\text{o}i}) \quad (2)$$

where $P_{\text{m}i}$ and $P_{\text{o}i}$ are the modelled and observed ith probability values, respectively, of each bin and n is the number of bins. BS is the mean squared error measure for probability forecasts (Brier 1950) and S_{score} calculates the cumulative minimum value between the observed and modelled distributions for each binned value, thereby measuring the overlap area between two PDFs (Perkins *et al.* 2007).

ANALYSES OF RESULTS

Model performance

Model biases of air temperature and precipitation for both mean and percentile values are shown in Figure 2. The mean value of model biases at all stations was about 0.5 °C for the simulated T_{max} and T_{min} during both calibration and validation periods. Figure 2 shows that NHMM tends to underestimate the three statistics of precipitation (dsl, wsl and wpa). Underestimation of dsl and wsl implies that the simulated wet or dry spell lengths are shorter than the observed durations. However, there is no significant difference between the simulated and observed precipitation, with the REs of the three precipitation statistics being less than 15%.

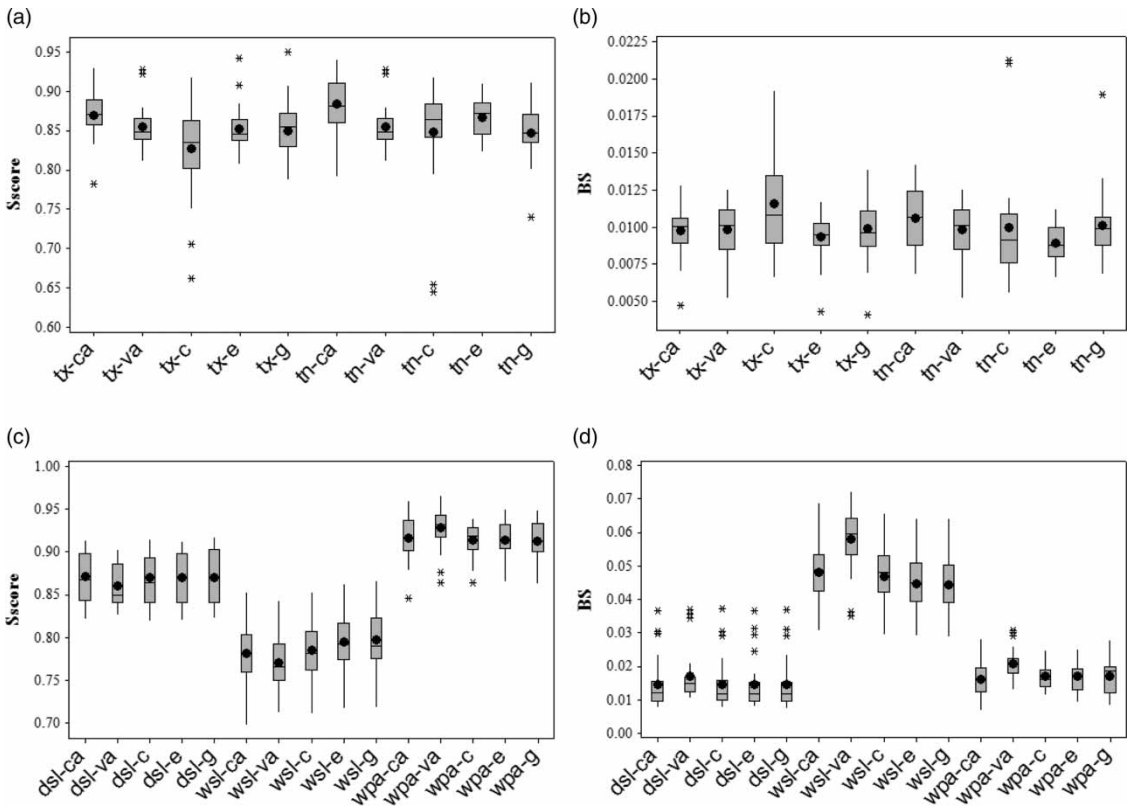

Figure 3 | Boxplots for precipitation, maximum and minimum air temperatures based on skill scores: (a), (b) air temperature and (c), (d) precipitation; *x*-axis notation as for Figure 2.

The results of the two PDF-based skill scores S_{score} and *BS* for air temperature and precipitation are shown in Figure 3. It can be seen from Figure 3 that NHMM more accurately simulated dsl than wsl in the TRB, with greater S_{score} values and lower *BS* values for dsl than for wsl. This might be because the dsl values are much higher than wsl in the arid region, and the SDSM is better able to model time series when using higher values. This result is consistent with from the findings of Liu, L. L. *et al.* (2011) and Liu, Z. F. *et al.* (2011). NHMM performed well in modelling wpa with S_{score} greater than 0.9 in both calibration and validation periods. SDSM also performed well in downscaling T_{max} and T_{min}, with S_{score} values at most stations greater than 0.8 in both calibration and validation periods. In general, both the SDSM and NHMM showed abilities to downscale daily precipitation, T_{max} and T_{min} over the TRB study area.

It can been seen from Figures 2 and 3 that there was little difference in the performance of the NHMM and SDSM between the calibration and validation periods, which indicated that both models demonstrate the ability to downscale the precipitation and air temperature in different time periods over the TRB. In addition, when NCEP predictors were replaced by GCM (CSIRO30, ECHAM5 and GFDL21) predictors in downscaling precipitation, T_{max} and T_{min} in the calibration period, there were no significant differences in model performance with only minor changes in the values of

Table 1 | Model performance on monthly runoff in calibration and validation periods

Period	Nash efficiency coefficient	Relative error (%)	Correlation coefficient
Calibration	0.821	6.3	0.894
Validation	0.782	8.1	0.877

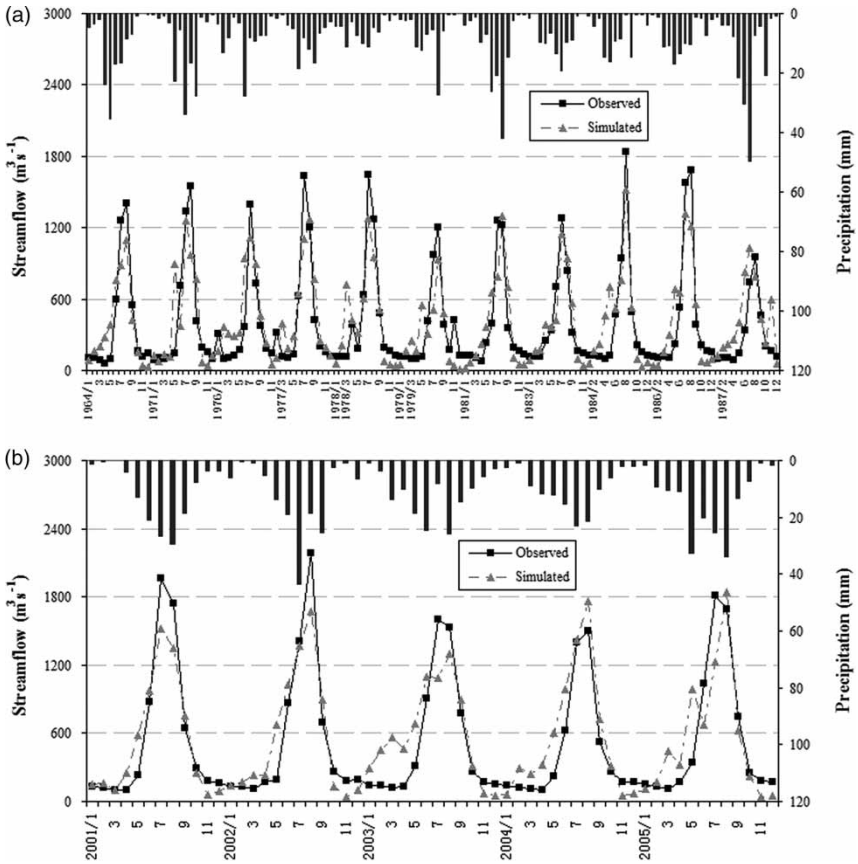

Figure 4 | Mean monthly hydrographs for calibration and validation periods in headwater catchment of the TRB ((a) and (b) describe hydrographs for calibration and validation periods, respectively).

S_{score} and BS. This indicated that the relationships between predictors and predicands calibrated by NCEP predictors could also be used as predictors in these three GCMs.

Comparisons between the simulated and observed flows for the calibration and validation periods are listed in Table 1 and shown in Figure 4. In general, both the simulated annual runoff volumes and the hydrograph shape were consistent with the observed values; for example, Nash & Sutcliffe (1970) reported efficiency coefficients for the model as 0.821 and 0.782 during calibration and validation periods, respectively. Streamflow was overestimated during all the simulated periods. Total runoff was well simulated in the catchment, with REs less than 10%. The correlation coefficient between the simulated and observed flows was greater than 0.87 for all simulated periods. Overall, the calibrated VIC-3L model showed satisfactory model performance in simulating the streamflow in the HC.

Local climate change scenarios

Figure 5 depicts the changes in mean values of monthly, seasonal and annual precipitation, T_{max} and T_{min} generated by the SDSMs. Changes in the annual precipitation projected by the SDSM were not obvious, with the changes being lesser than 15% under all combined scenarios. The magnitude of annual precipitation change during the period 2081–2100 was smaller than that during 2046–2065. In both periods, CSIRO30 tended to project increasing trends for annual precipitation, while ECHAM5 and GFDL21 projected decreasing trends under all three combined scenarios. The predictions for monthly precipitation showed much greater changes than annual precipitation based on the SDSM, ranging from approximately –80 to 60%. Note that the monthly precipitation showed increasing trends only in March and July under most combined scenarios for the period 2046–2065. Monthly precipitation exhibited

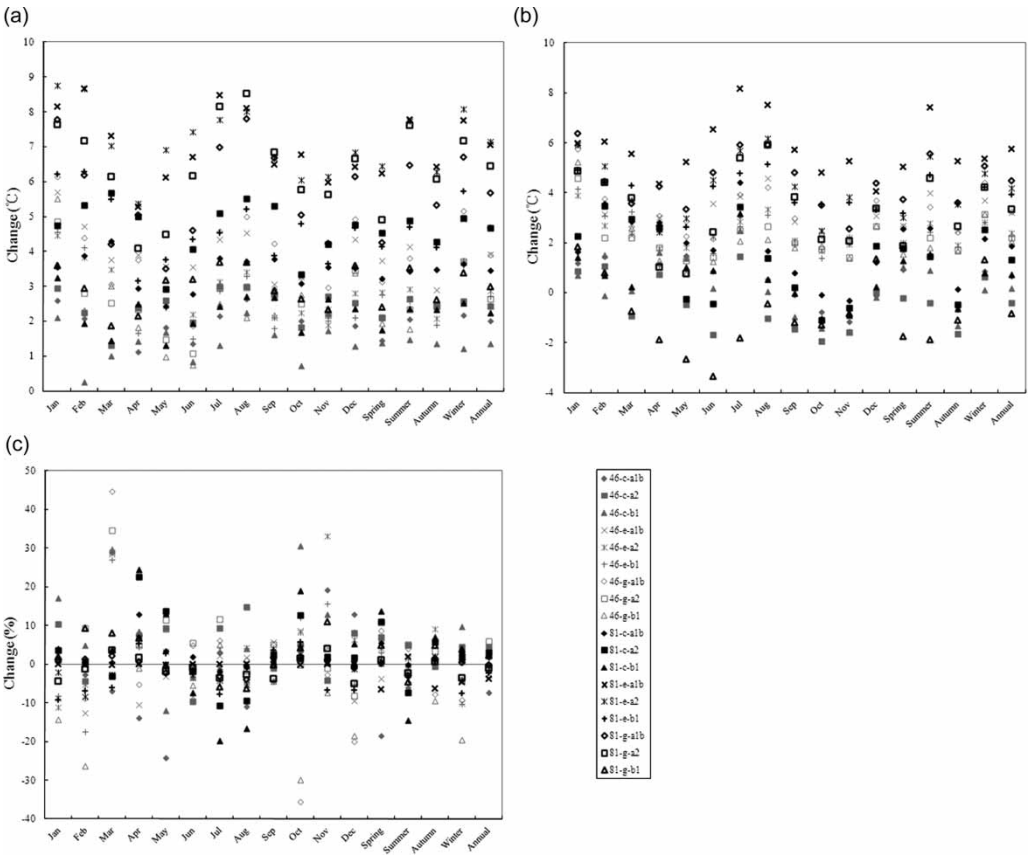

Figure 5 | Changes of mean values for (a) maximum air temperature, (b) minimum air temperature and (c) precipitation projected by statistical downscaling models. 46, 81 refer to the periods of 2046–2065 and 2081–2100, respectively; a1b, a2 and b1 refer to SRES A1B, A2 and B1, respectively.

increasing trends in April, May, October and November, with decreasing trends in July and August under all combined scenarios for the period of 2081–2100. Changes in monthly precipitation for the period 2081–2100 were also smaller than those for the period 2046–2065.

Figure 5(a) shows that T_{max} exhibited increasing trends under all combined scenarios. The predicted increase was greater during 2081–2100 than during 2046–2065, with the greatest change exceeding 7.0 °C. The magnitude of the increasing trend was greatest under the A2 scenario and was the smallest under the B1 scenario, with the A1B scenario inbetween. In both periods, the increasing trend of T_{max} projected by CSIRO30 was smaller than that by ECHAM5 and GFDL21. The difference between changes in monthly and annual T_{max} was not as obvious as that for precipitation.

Figure 5(b) shows that T_{min} exhibited increasing trends under most combined scenarios, except for CSIRO30-related scenarios and the combined GFDL21-B1 scenario. Changes in annual T_{min} ranged from –0.4 to 3.3 °C in the period 2046–2065 and ranged from –0.9 to 5.9 °C during 2081–2100. The difference between changes in monthly and annual T_{min} was not as obvious as that for precipitation. Notably, the winter T_{min} showed increasing trends under all combined scenarios for both periods, which may result in greater snowmelt runoff in the HC.

Impact of climate change on monthly runoff

Daily meteorological data at each station, generated by downscaling models, were input to the calibrated VIC-3L model to simulate hydrological processes under climate change scenarios in the study area.

Monthly, seasonal and annual changes for runoff at the HC, which is controlled by the Alar station, are shown in Figure 6. Driven by different combined climate change scenarios, annual runoff for the HC was predicted to vary by –20.7 to 4.9% during the period 2046–2065 and by 0.5–7.2% during 2081–2100. In general, the predictions did not show an obvious change for annual runoff, with the magnitude of these changes being less than 8% in most of the combined climate change scenarios. Predicted runoff showed greater changes under SRES A2 than the A1B and B1.

Although there was little change in annual runoff driven by climate change scenarios at the HC, the results showed more obvious changes (up to almost 70%) for monthly and seasonal runoff for the 2046–2065 period. Runoff showed the greatest change under the A2 scenario and the smallest change under the B1 scenario. The greatest and smallest changes were observed for the ECHAM5 and CSIRO30 models, respectively. There was a decreasing trend for the months June–August (summer) and increasing trends for October–February (winter). Monthly and seasonal runoff changes predicted for 2081–2100 differed from those for 2046–2065. For the period 2081–2100, there was an increasing trend in seasonal runoff except for summer runoff, in which winter runoff increased most (exceeding 20%). Monthly runoff changed by less than 10% under most combined climate change scenarios, except in November–January of the following year in which the changes in the monthly runoff were higher than 20%. Although there was

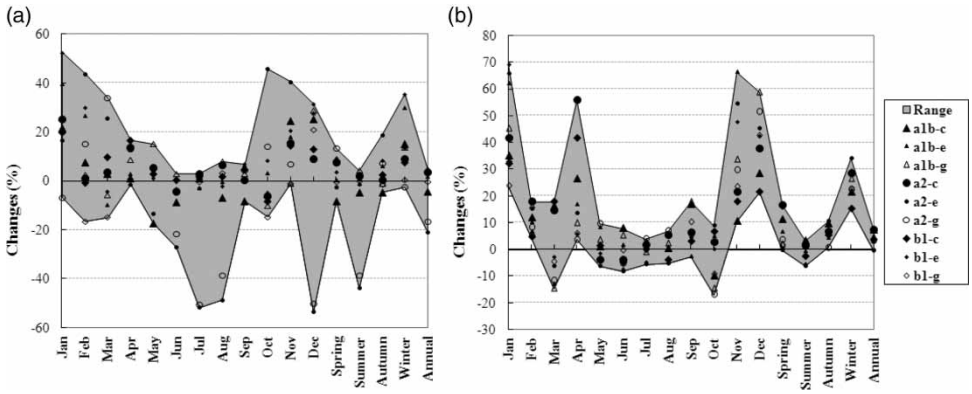

Figure 6 | Monthly, seasonal and annual runoff changes under climate change scenarios in the future for (a) 2046–2065 and (b) 2081–2100.

a relatively large change in the runoff for November–January, the increased water volume was not so great because it was in low-flow seasons. In both periods, there was an obviously increasing trend of the runoff in April (which might be beneficial to agricultural irrigation in spring). Monthly and seasonal runoff changed more under A2 and A1B than under B1, while there was little overall difference among the three GCMs.

Although the results showed a decreasing trend for precipitation during June–August (summer), runoff in these months tended to increase during the period of 2081–2100 (Figure 5). In addition, there were decreasing trends for precipitation in the period November– January (Figure 5), whereas runoff exhibited obviously increasing trends. For example, it can be seen from Figure 7 that runoff increased by more than 20% in January, while corresponding precipitation showed a minor reduction of less than 3% and even decreased by more than 10% under some combined climate change scenarios. The overall outcome of increased runoff despite reduced precipitation might be due to increased snowmelt runoff due to increased air temperature.

Impact of climate change on spatial distribution of runoff

Figure 8 shows spatial distributions of runoff changes in the HC during the period 2046–2065, compared with the benchmark period (1981–2000). Driven by climate change scenarios, runoff in the period 2046–2065 is predicted to vary by between –50 and +50% compared to the benchmark period. Runoff showed an obviously decreasing trend under the A1B scenario, especially under the combined GFDL21-A1B scenario in which the decreasing trend area exceeded 80% of the entire study region and 33% of the entire region was predicted to experience more than 25% reduction. Runoff tends to increase under the A2 scenario, especially under the combined ECHAM5-A2 scenario which predicted an increasing trend in almost 75% of the area of the entire study region. This scenario showed an obviously increasing runoff trend in the upstream regions of the Akesu and Yerqiang rivers, with most regions showing more than 25% more runoff. That outcome was beneficial to the total runoff for the HC, because runoff at upstream regions comprises most of the total runoff. Although there was little obvious change in runoff under the combined CSIRO30-B1 scenario, there was an obviously decreasing trend under the combined ECHAM5-B1 and GFDL21-B1 scenarios in which spatial distributions were similar to that under the A1B scenario.

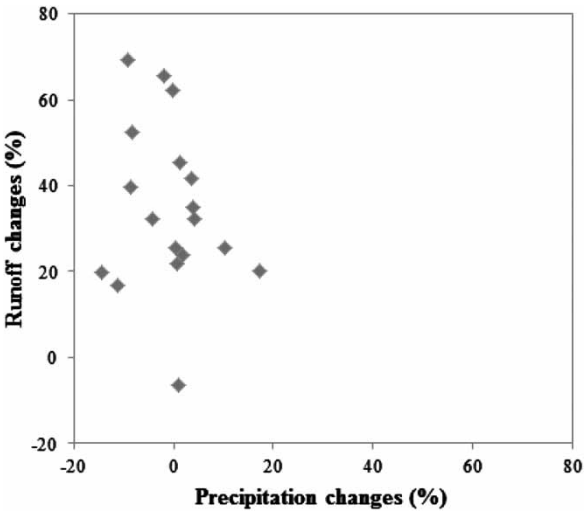

Figure 7 | Scatter plot for runoff and precipitation changes in January.

Overall, runoff in the HC during the period 2046–2065 tends to decrease compared with the benchmark period because the results showed more combined scenarios with decreasing than increasing trends. Predictions were more consistent for spatial distributions of runoff under the same GCM than results under the same emission scenario. In other words, the impact of different GCMs on spatial distribution of runoff might be more significant than that of differing emission scenarios. Runoff at the Akesu River catchment decreased under most climate change scenarios except for A2, while runoff at the Yerqiang and Hetian river catchments increased under some combined scenarios and exhibited decreasing trends under other combined scenarios.

Impact of climate change on spatial distribution of evapotranspiration

Figure 9 describes spatial distribution of evapotranspiration changes in the HC during the period 2046–2065, compared with the benchmark period. There were obvious changes in the spatial distribution of

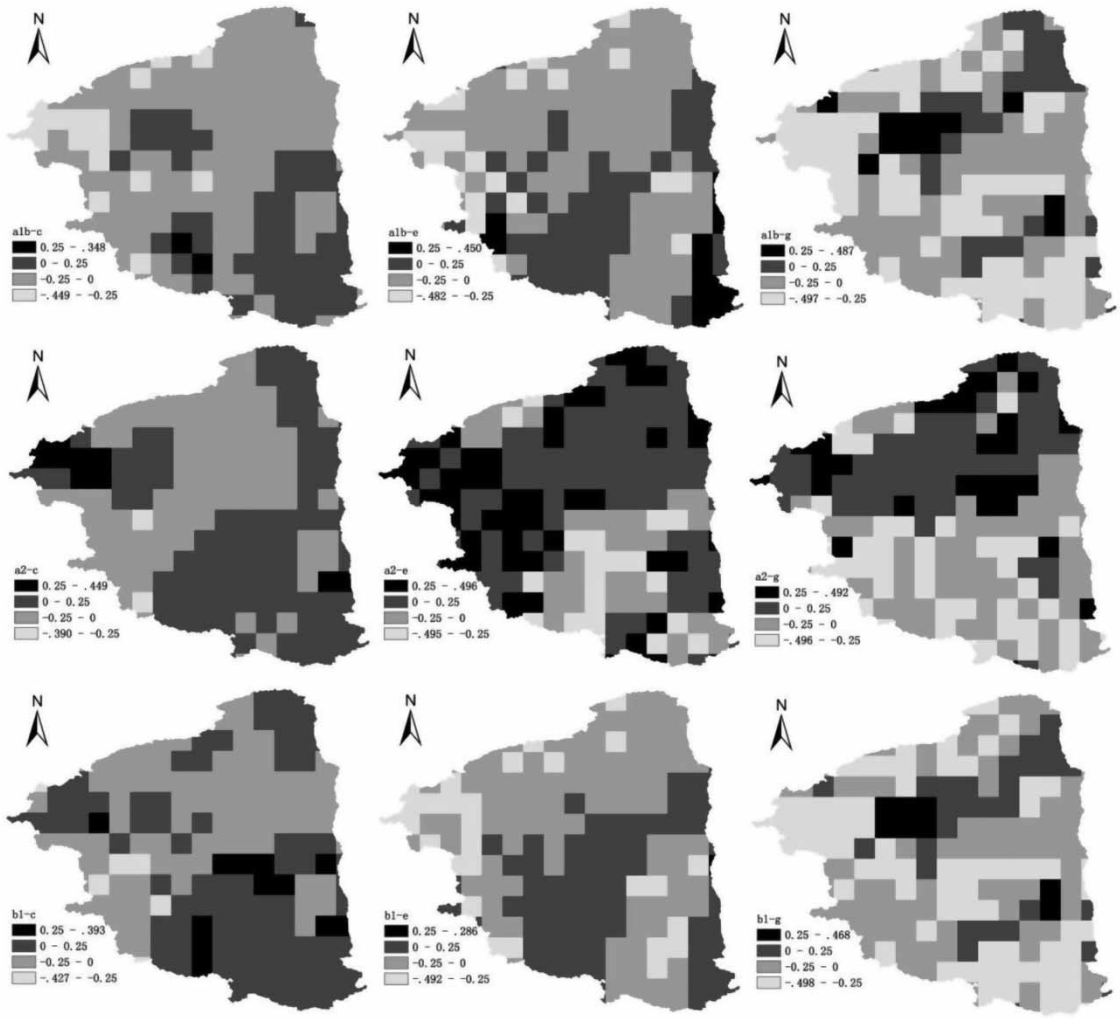

Figure 8 | Spatial distribution of runoff changes in the headwater catchment during the period 2046–2065.

evapotranspiration. The maximum variation ranged from –50 to 80%, which was predicted under the combined GFDL21-A2 scenario. The minimum changes in evapotranspiration were observed under the combined CSIRO-A2 scenario (ranging from –2 to 18.3%). In general, evapotranspiration in most regions of the HC changed from –20 to 40% under combined climate change scenarios for the period 2046–2065, and the area demonstrating an increasing trend was larger than that demonstrating a decreasing trend. The results also showed more consistent spatial distributions of evapotranspiration under a GCM than under a particular emission scenario. For example, when evapotranspiration was driven by climate change GFDL21 scenarios, the results always showed the maximum increasing evapotranspiration at the northern region with an increasing trend larger than 36% and a maximum decreasing trend at the upstream regions of the Yerqiang and Hetian rivers. The results also showed the maximum increasing trend at the northern region when evapotranspiration was driven by climate change scenarios of ECHAM5, but exhibited maximum decreasing trend at the downstream region of the Akesu and Yerqiang rivers with the magnitude of these trends being smaller than for GFDL21. The increasing trend of evapotranspiration at the northwest region was greater than that for other regions.

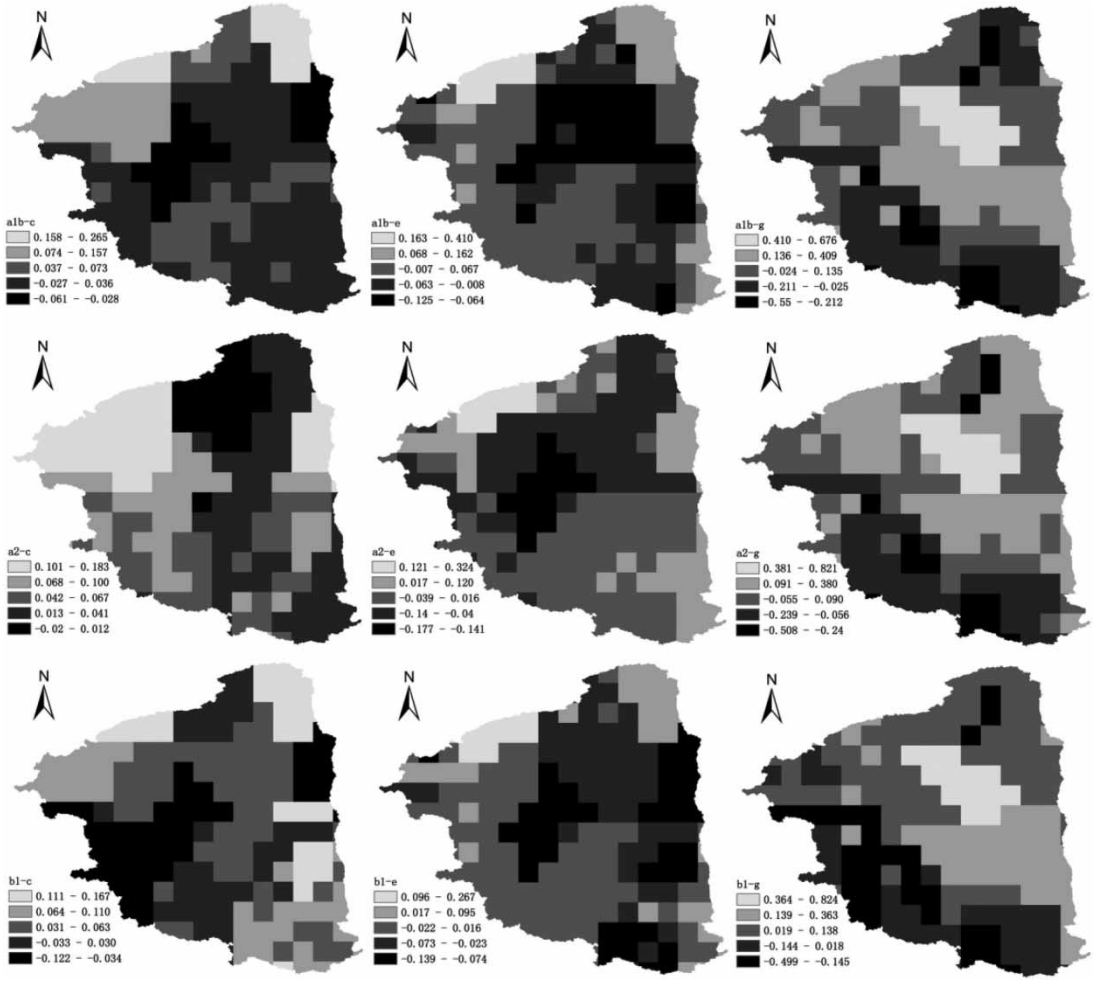

Figure 9 | Spatial distribution of evapotranspiration changes in the headwater catchment during the period 2046–2065.

DISCUSSION AND CONCLUSIONS

Regional climate change scenarios, statistically downscaled from the outputs of three GCMs and three IPCC Special Report on Emission Scenarios (SRES A1B, A2 and B1), were used to assess the impact of climate change on hydrological processes in the HC of the TRB.

The results showed an obvious increasing trend for minimum and maximum air temperatures in the TRB under nine combined scenarios in which the magnitude of the increasing trend was the greatest under SRES A2, smallest under SRES B1 and intermediate under SRES A1B. This was consistent with the changes in air temperature under different emission scenarios around the world. The results exhibit a decreasing trend for precipitation in the HC, with the magnitude of decreasing trend being less than 10% at all stations; the magnitude was less than 5% at most stations. The magnitude of the increasing air temperature in the period 2081–2100 was greater than that for the period 2046–2065, while the magnitude of changes in the annual precipitation for 2081–2100 was lower than that for 2046–2065. The trends for air temperature and precipitation are different; the magnitude of changes in the extreme values of precipitation is remarkably greater than that of the changes in the mean values of precipitation.

Runoff in the HC tended to exhibit a decreasing trend under future climate change scenarios, but showed

an increasing trend for winter runoff which was mainly attributed to increased snowmelt runoff resulting from warmer winters. This finding was consistent with the findings reported in previous studies (e.g. Boyer *et al.* 2010; Chang & Jung 2010; Chen *et al.* 2011; Forbes *et al.* 2011; Liu, L. L. *et al.* 2011; Liu, Z. F. *et al.* 2011; Kienzle *et al.* 2012). In the case of the HC, both precipitation and runoff showed an obviously increasing trend in April. This might be beneficial for spring irrigation in the study area. The spatial distribution of runoff under different GCMs was more consistent with that under different emission scenarios. This suggests that the impact of different GCM outputs on the spatial distribution of runoff was more significant than that of various emission scenarios; this was consistent with previous studies and demonstrates that uncertainty levels associated with GCM outputs are the most important factor in assessing the impact of climate change. The results show an inconsistent intra-annual distribution of the changes in precipitation and runoff in the HC; this distribution may be explained by the increased snowmelt runoff resulting from the increasing air temperature.

ACKNOWLEDGEMENTS

This study is jointly financed by the National Natural Science Foundation of China (No. 41161008) and Key Direction Project of Innovation Program (KZCX2-YW-127). Thanks are also extended to the Chinese Scholarship Council-CSIRO Joint Supervision of Chinese PhD student project, which has enabled the first author to study in Australia for 1 year.

REFERENCES

Abdo, K. S., Fiseha, B. M., Rjentjes, T. H. M., Gieske, A. S. M. & Haile, A. T. 2009 Assessment of climate change impacts on the hydrology of Gilgel Abay catchment in Lake Tana basin, Ethiopia. *Hydrological Processes* **23**, 3661–3669.

Andersson, L., Samuelsson, P. & Kjellström, E. 2011 Assessment of climate change impact on water resources in the Pungwe river basin. *Tellus* **63A** (1), 138–157.

Bae, D. H., Jung, I. W. & Lettenmaier, D. P. 2011 Hydrologic uncertainties in climate change from IPCC AR4 GCM simulations of the Chungju Basin, Korea. *Journal of Hydrology* **401**, 90–105.

Bastola, S., Murphy, C. & Sweeney, J. 2011 The role of hydrological modelling uncertainties in climate change impact assessments of Irish river catchments. *Advances in Water Resources* **34**, 562–576.

Beyene, T., Lettenmaier, D. P. & Kabat, P. 2010 Hydrologic impacts of climate change on the Nile River Basin-implications of the 2007 IPCC scenarios. *Climatic Change* **100**, 433–461.

Boyer, C., Chaumont, D., Chartier, I. & Roy, A. G. 2010 Impact of climate change on the hydrology of St. Lawrence tributaries. *Journal of Hydrology* **384**, 65–83.

Brier, G. W. 1950 Verification of forecasts expressed in terms of probability. *Monthly Weather Review* **78**, 1–3.

Cavazos, T. & Hewitson, B. C. 2005 Performance of NCEP-NCAR reanalysis variables in statistical downscaling of daily precipitation. *Climate Research* **28**, 95–107.

Chang, H. & Jung, I. W. 2010 Spatial and temporal changes in runoff caused by climate change in a complex large river basin in Oregon. *Journal of Hydrology* **388**, 186–207.

Charles, S. P., Bates, B. C. & Hughes, J. P. 1999 A spatiotemporal model for downscaling precipitation occurrence and amounts. *Journal of Geophysical Research* **104** (D24), 31657–31669.

Chen, J., Brissette, F. P. & Leconte, R. 2011 Uncertainty of downscaling method in quantifying the impact of climate change on hydrology. *Journal of Hydrology* **401**, 190–202.

Chen, Y. N., Takeuchi, K., Xu, C. C., Chen, Y. P. & Xu, Z. X. 2006 Regional climate change and its effects on river runoff in the Tarim Basin, China. *Hydrological Processes* **20**, 2207–2216.

Chiew, F. H. S., Kirono, D. G. C., Kent, D. M., Frost, A. J., Charles, S. P., Timbal, B., Nguyen, K. C. & Fu, G. B. 2010 Comparison of runoff modelled using rainfall from different downscaling methods for historical and future climates. *Journal of Hydrology* **387**, 10–23.

Christensen, J. H., Hewitson, B., Busuioc, A., Chen, A., Gao, X., Held, I., Jones, R., Kolli, R. K., Kwon, W. T., Laprise, R., Magaña, R. V., Mearns, L., Menéndez, C. G., Räisänen, J., Rinke, A., Sarr, A. & Whetton, P. 2007 Regional climate projections. In: S. Solomon, D. Qin, M. Manning, Z. Chen, M. Marquis, K. B. Avery, M. Tignor & H. L. Miller (eds), *Climate Change 2007: The Physical Science Basis*. Contribution of Working Group I to the Fourth Assessment Report of the Intergovernmental Panel on Climate Change. Cambridge University Press, Cambridge.

Cubasch, U., von Storch, H., Waszkewitz, J. & Zorita, E. 1996 Estimates of climate change in Southern Europe derived from dynamical climate model output. *Climate Research* **7**, 129–149.

Elsner, M. M., Cuo, L., Voisin, N., Deems, J. S., Hamlet, A. F., Vano, J. A., Mickelson, K. E. B., Lee, S. Y. & Lettenmaier, D. P. 2010 Implications of 21st century climate change for the hydrology of Washington State. *Climatic Change* **102**,

225–260. http://www.springerlink.com/content/84613v872p102578/.

Forbes, K. A., Kienzle, S. W., Coburn, C. A., Byrne, J. M. & Rasmussen, J. 2011 Simulating the hydrological response to predicted climate change on a watershed in southern Alberta, Canada. *Climatic Change* **105**, 555–576.

Fowler, H. J., Blenkinsop, S. & Tebaldi, C. 2007 Linking climate modeling to impacts studies: recent advances in downscaling techniques for hydrological modeling. *International Journal of Climatology* **27**, 1547–1578.

Gleick, P. H. 1986 Methods for evaluating the regional hydrologic impacts of global climatic change. *Journal of Hydrology* **88**, 97–116.

Graham, L. P., Andersson, L., Horan, M., Kunz, R., Lumsden, T., Schulze, R., Warburton, M., Wilk, J. & Yang, W. 2011 Using multiple climate projections for assessing hydrological response to climate change in the Thukela River Basin, South Africa. *Physics and Chemistry of the Earth* **36** (14–15), 727–735.

Hagg, W., Shahgedanova, M., Mayer, C., Lambrecht, A. & Popovnin, V. 2010 A sensitivity study for water availability in the Northern Caucasus based on climate projections. *Global Planetary Change* **73**, 161–171.

Harpham, C. & Wilby, R. L. 2005 Multi-site downscaling of heavy daily precipitation occurrence and amounts. *Journal of Hydrology* **312**, 235–255.

Jiang, T., Chen, Y. Q., Xu, C. Y., Chen, X. H., Chen, X. & Singh, V. P. 2007 Comparison of hydrological impacts of climate change simulated by six hydrological models in the Dongjiang Basin, South China. *Journal of Hydrology* **336**, 316–333.

Kalnay, E., Kanamitsu, M., Kistler, R., Collins, W., Deaven, D., GandIn, L., Iredell, M., Saha, S., White, G., Woollen, J., Zhu, Y., Chelliah, M., Ebisuzaki, W., Higgins, W., Janowiak, J., Mo, K. C., Ropelewski, C., Wang, J., Leetmaa, A., Reynolds, R., Jenne, R. & Joseph, D. 1996 The NCEP/NCAR 40–Year Reanalysis Project. *Bulletin of the American Meteorological Society* **77** (3), 437–471.

Karl, T. R., Wang, W. C., Schlesinger, M. E., Knight, R. W. & Portman, D. 1990 A method of relating general circulation model simulated climate to observed local climate. Part I: Seasonal statistics. *Journal of Climate* **3**, 1053–1079.

Kehta, N., Elshorbagy, A. & Carey, S. 2012 Impacts of climate change on soil moisture and evapotranspiration in reconstructed watersheds in northern Alberta, Canada. *Hydrological Processes* **26** (9), 1321–1331.

Khazaei, M. R., Zahabiyoun, B. & Saghafian, B. 2011 Assessment of climate change impact on floods using weather generator and continuous rainfall-runoff model. *International Journal of Climatology*. DOI: 10.1002/joc.2416.

Kienzle, S. W., Nemeth, M. W., Byrne, J. M. & MacDonald, R. J. 2012 Simulating the hydrological impacts of climate change in the upper North Saskatchewan River basin, Alberta, Canada. *Journal of Hydrology* **412–413** (4), 76–89.

Kistler, R., Kalnay, E., Collins, W., Saha, S., White, G., Woollen, J., Chelliah, M., Ebisuzaki, W., Kanamitsu, V., Kousky, M., van den Dool, H., Jenne, R. & Fiorino, M. 2001 The NCEP/NCAR 50–year reanalysis. *Bulletin of the American Meteorological Society* **82**, 247–267.

Lan, C., Beyene, T. K., Voisin, N., Su, F. G., Lettenmaier, D. P., Alberti, M. & Richey, J. E. 2011 Effects of mid-twenty-first century climate and land cover change on the hydrology of the Puget Sound basin, Washington. *Hydrological Processes* **25**, 1729–1753.

Liang, X. & Xie, Z. H. 2001 A new surface runoff parameterization with subgrid-scale soil heterogeneity for land surface models. *Advances in Water Resources* **24**, 1173–1193.

Liang, X., Lettenmaier, D. P., Wood, E. F. & Burges, S. J. 1994 A simple hydrologically based model of land surface water and energy fluxes for general circulation models. *Journal of Geophysical Research* **99** (D7), 14415–14428.

Liang, X., Lettenmaier, D. P. & Wood, E. F. 1996 One-dimensional statistical dynamic representation of subgrid spatial variability of precipitation in the two-layer variable infiltration capacity model. *Journal of Geophysical Research* **101**, 21403–21422.

Liu, L. L., Liu, Z. F., Ren, X. Y., Fischer, T. & Xu, Y. 2011 Hydrological impacts of climate change in the Yellow River Basin for the 21st century using hydrological model and statistical downscaling model. *Quaternary International* **244** (2), 211–220.

Liu, Z. F., Xu, Z. X., Charles, S. P., Fu, G. B. & Liu, L. 2011 Evaluation of two statistical downscaling models for daily precipitation over an arid basin in China. *International Journal of Climatology* **31** (13), 2006–2020.

Liu, Z. F., Xu, Z. X., Huang, J. X., Charles, S. P. & Fu, G. B. 2010 Impacts of climate change on hydrological processes in headwater catchment of the Tarim River Basin. *Hydrological Processes* **24**, 196–208.

Maurer, E. P., Brekke, L. D. & Pruitt, T. 2010 Contrasting lumped and distributed hydrology models for estimating climate change impacts on California watersheds. *Journal of American Water Resources Association* **46** (5), 1024–1035.

McAvaney, B., Covey, C., Joussaume, S., Kattsov, V., Kitoh, A., Ogana, W., Pitman, A., Weaver, A., Wood, R. & Zhao, Z. C. 2001 *Climate Change 2001: The Scientific Basis, Chap. 8: Model Evaluation*. Cambridge University Press, Cambridge and New York.

Meng, D. J. & Mo, X. G. 2012 Assessing the effect of climate change on mean annual runoff in the Songhua River basin, China. *Hydrological Processes* **26** (7), 1050–1061.

Murphy, J. M. 1999 An evaluation of statistical and dynamical techniques for downscaling local climate. *Journal of Climate* **12**, 2256–2284.

Murphy, J. M., Sexton, D. M. H., Barnett, D. N., Jones, G. S., Webb, M. J., Collins, M. & Stainforth, D. A. 2004 Quantification of modelling uncertainties in a large ensemble of climate change simulations. *Nature* **430**, 768–772.

Nash, J. E. & Sutcliffe, J. V. 1970 River flow forecasting through conceptual models part 1: a discussion of principles. *Journal of Hydrology* **10**, 282–290.

Perkins, S. E., Pitman, A. J., Holbrook, N. J. & Mcaneney, J. 2007 Evaluation of the AR4 climate models' simulated daily

maximum air temperature, minimum air temperature, and precipitation over Australia using probability density functions. *Journal of Climate* **20**, 4356–4376.

Prudhomme, C. & Davies, H. 2009 Assessing uncertainties in climate change impact analyses on the river flow regimes in the UK. Part 1, baseline climate. *Climatic Change* **93**, 177–195.

Schubert, S. 1998 Downscaling local extreme temperature changes in south-eastern Australia from the CSIRO Mark2 GCM. *International Journal of Climatology* **18**, 1419–1438.

Singh, P. & Kumar, N. 1997 Impact assessment of climate change on the hydrological response of a snow and glacier melt runoff dominated Himalayan river. *Journal of Hydrology* **193**, 316–350.

Solomon, S., Qin, D., Manning, M., Alley, R. B., Berntsen, T., Bindoff, N. L., Chen, Z., Chidthaisong, A., Gregory, J. M., Hegerl, G. C., Heimann, M., Hewitson, B., Hoskins, B. J., Joos, F., Jouzel, J., Kattsov, V., Lohmann, U., Matsuno, T., Molina, M., Nicholls, N., Overpeck, J., Raga, G., Ramaswamy, V., Ren, J., Rusticucci, M., Somerville, R., Stocker, T. F., Whetton, P., Wood, R. A. & Wratt, D. 2007 Technical summary. In: *Climate Change 2007: The Physical Science Basis* (S. Solomon, D. Qin, M. Manning, Z. Chen, M. Marquis, K. B. Averyt, M. Tignor & H. L. Miller, eds). Cambridge University Press, Cambridge and New York.

Sosa, J. M. R., Brandani, G., Dibari, C., Moriondo, M., Ferrise, R., Trombi, G. & Bindi, M. 2011 Climate change impact on the hydrological balance of the Itaipu Basin. *Meteorological Applications* **18**, 163–170.

Su, F. & Xie, Z. 2003 A model for assessing effects of climate change on runoff of in China. *Progress in Natural Science* **13** (9), 701–707.

Teegavarapu, R. S. V. 2010 Modeling climate change uncertainties in water resources management models. *Environmental Modelling and Software* **25**, 1261–1265.

Teutschbein, C., Wetterhall, F. & Seibert, J. 2011 Evaluation of different downscaling techniques for hydrological climate-change impact studies at the catchment scale. *Climate Dynamics* **37**, 2087–2105.

Timbal, B., Dufour, A. & McAvaney, B. 2003 An estimate of future climate change for western France using a statistical downscaling technique. *Climate Dynamics* **20**, 807–823.

Wilby, R. L. & Wigley, T. M. L. 2000 Precipitation predictors for downscaling: observed and general circulation model relationships. *International Journal of Climatology* **20**, 641–661.

Wilby, R. L., Hay, L. E., Gutowski, W. J. J., Arritt, R. W., Takle, E. S., Pan, Z., Leavesley, G. H. & Clark, M. P. 2000 Hydrological responses to dynamically and statistically downscaled climate model output. *Geophysical Research Letters* **27**, 1199–1202.

Wilby, R. L., Dawson, C. W. & Barrow, E. M. 2002 SDSM – a decision support tool for the assessment of regional climate change impacts. *Environmental Modelleling and Software* **17**, 147–159.

Wilby, R. L., Charles, S. P., Zorita, E., Timbal, B., Whetton, P. & Mearns, L. O. 2004 Guidelines for use of climate scenarios developed from statistical downscaling methods. Supporting material of the Intergovernmental Panel on Climate Change (IPCC), prepared on behalf of Task Group on Data and Scenario Support for Impacts and Climate Analysis (TGICA). http://www.narccap.ucar.edu/doc/tgica-guidance-2004.pdf (accessed September 2012).

Wood, A. W., Leung, L. R., Sridhar, V. & Lettenmaier, D. P. 2004 Hydrologic implications of dynamical and statistical approaches to downscaling climate model outputs. *Climatic Change* **62**, 189–216.

Xie, Z. H., Liu, Q. & Su, F. G. 2004 An application of the VIC-3L land surface model with the new surface runoff model in simulating streamflow for the Yellow River basin. *IAHS Publication* **289**, 241–248.

Xu, C. Y. 1999 From GCMs to river flow: a review of downscaling techniques and hydrologic modeling approaches. *Progress in Physical Geography* **23** (2), 229–249.

Xu, Z. X., Liu, Z. F., Fu, G. B., Chen, Y. N. & Huang, J. X. 2010 Trends of major hydroclimatic variables in the Tarim River basin during the past 50 years. *Journal of Arid Environments* **74**, 256–267.

Ye, X. C., Zhang, Q., Bai, L. & Hu, Q. 2011 A modeling study of catchment discharge to Poyang Lake under future climate in China. *Quaternary International* **244** (2), 221–229.

Zeng, X. F., Kundzewicz, Z. W., Zhou, J. Z. & Su, B. D. 2011 Discharge projection in the Yangtze River basin under different emission scenarios based on the artificial neural networks. *Quaternary International*. DOI:10.1016/j.quaint.2011.06.009.

Zhang, Q., Xu, C. Y., Tao, H., Jiang, T. & Chen, Y. D. 2010 Climate changes and their impacts on water resources in the arid regions – a case study of the Tarim River basin, China. *Stochastic Environmental Research and Risk Assessment* **24**, 349–358.

First received 8 October 2011; accepted in revised form 24 February 2012. Available online 9 October 2012